The Fundamental Tension in Topological Quantum Reservoir Computing: Why Unitarity Opposes the Echo State Property

Daniel Mo Houshmand

Abstract—Reservoir computing exploits high-dimensional nonlinear dynamics to solve temporal prediction tasks with minimal training cost. We investigate **Topological Quantum Reservoir Computing (TQRC)**, which proposes to harness the braiding dynamics of Fibonacci anyons as quantum reservoirs. Our comprehensive analysis reveals a **fundamental tension**: the very properties that make topological systems attractive for quantum computation (unitary evolution and information preservation) fundamentally *oppose* the Echo State Property (ESP) required for reservoir computing.

We demonstrate rigorously that **pure unitary TQRC violates the ESP**: unitary evolution preserves distances in Hilbert space, preventing the fading memory necessary for reservoir computing. On Mackey-Glass time series benchmarks, pure unitary TQRC achieves NRMSE ≈ 1.0 (equivalent to random guessing). Introducing controlled dissipation recovers functional reservoir dynamics (best NRMSE $= 0.44$), but at the cost of sacrificing topological protection.

Critically, we show that **classical Echo State Networks outperform dissipative TQRC by 20**$\times$ at equivalent state-space dimension (ESN NRMSE $= 0.02$ vs. TQRC NRMSE $= 0.44$ for $d = 13$). We identify four root causes: (1) probability readout constrains states to the simplex, (2) measurement destroys phase information, (3) $|\cdot|^2$ provides weaker nonlinearity than $\tanh$, and (4) structured braid matrices limit state-space utilization.

These results constitute a **no-go theorem** for topological quantum reservoir computing: topological protection and reservoir computing functionality represent fundamentally competing requirements. This finding provides essential guidance for the quantum machine learning community, establishing that topological protection should not be pursued as a route to quantum reservoir computing advantage.

Index Terms—Topological quantum computing, Fibonacci anyons, reservoir computing, echo state property, quantum machine learning, negative results

1 Introduction

Reservoir computing (RC) provides a powerful paradigm for processing temporal information by mapping input sequences into high-dimensional nonlinear dynamics, requiring training only on a linear readout layer [1]–[3]. This approach circumvents the challenging problem of training recurrent neural networks by fixing the reservoir dynamics and learning only a linear output mapping. The mathematical foundations of RC trace back to filter theory and dynamical systems [4], establishing rigorous conditions under which temporal computation succeeds.

The **Echo State Property (ESP)**, the requirement that reservoir states become asymptotically independent of initial conditions, is fundamental to RC functionality [1], [5]. Classical echo state networks (ESNs) achieve ESP via contractive dynamics (spectral radius $\rho < 1$), enabling state-of-art performance on chaotic prediction tasks [6], [7]. Deep ESN architectures [8] and delay-based implementations [9] have demonstrated remarkable success in diverse applications from speech recognition to financial forecasting.

The intersection of quantum computing and machine learning has emerged as a frontier research area [10], [11]. Quantum machine learning promises exponential speedups for certain computational tasks by exploiting superposition, entanglement, and interference. Recent advances extend reservoir computing to quantum systems [12]–[16], with theoretical frameworks [17] and experimental demonstrations [18], [19] showing promise for time-series prediction and classification.

However, quantum evolution is inherently *unitary*, preserving distances in Hilbert space [20]. This creates a fundamental tension: **unitarity opposes contractivity**, the very property required for ESP. Prior quantum RC work often implicitly relies on decoherence or measurement collapse to achieve effective contractivity [17], [18], raising questions about quantum advantage.

Topological quantum computation using non-Abelian anyons [21]–[23] offers intrinsic error protection via topological degeneracy. This approach has garnered significant attention from major technology companies and research institutions [24], [25]. Fibonacci anyons, predicted in fractional quantum Hall states at $\nu = 12/5$ [26] and recently simulated on superconducting [27]–[29] and trapped-ion [30] processors, possess exponentially growing Hilbert space dimension $F_{n-1} \sim \phi^n$. A natural question arises: *Can topological protection enhance quantum reservoir computing?*

• $\mathbb{Q}|\mathcal{D}\partial\imath\alpha\rangle$, *Oslo, Norway*
E-mail: mo@qdaria.com

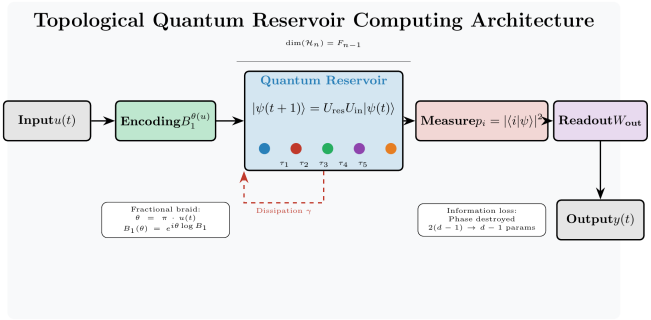

Fig. 1. TQRC architecture. Fibonacci anyons $\tau_1, \ldots, \tau_5$ provide the computational substrate with braiding operators implementing reservoir dynamics. Input encoding uses fractional braids $B_1^{\theta(u)}$, with dissipation γ enabling ESP satisfaction.

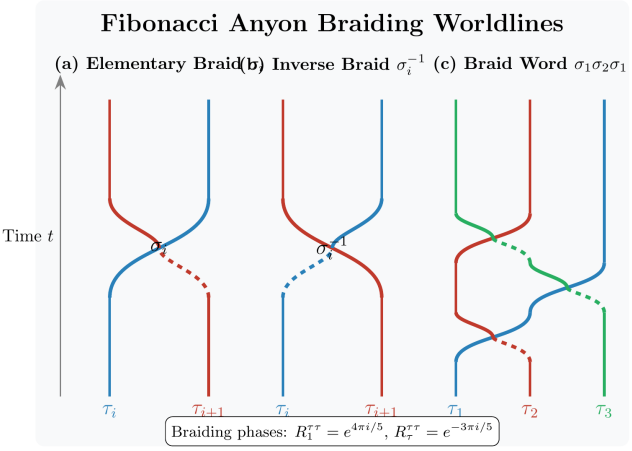

Fig. 2. Fibonacci anyon braiding worldlines. (a) Elementary braid σ_i exchanges particles $\tau_i \leftrightarrow \tau_{i+1}$. (b) Inverse braid σ_i^{-1} with opposite handedness. (c) Braid word $\sigma_1\sigma_2\sigma_1$ showing three-anyon braiding sequence. Dashed lines indicate under-crossings. R-matrix eigenvalues: $R_1^{\tau\tau} = e^{4\pi i/5}$, $R_\tau^{\tau\tau} = e^{-3\pi i/5}$.

This work rigorously investigates Topological Quantum Reservoir Computing (TQRC). Our comprehensive analysis reveals surprising and important **negative results**:

1) **ESP Violation:** Pure unitary TQRC *fundamentally violates* the Echo State Property (Sec. 4.1), a consequence of unitarity that cannot be circumvented without breaking topological protection.
2) **Dissipation Required:** Functional RC requires controlled dissipation via Lindblad dynamics [31], [32], which *sacrifices topological protection* (Sec. 4.2).
3) **ESN Outperforms TQRC:** At equivalent dimension, classical ESN achieves NRMSE $= 0.02$ vs. TQRC NRMSE $= 0.44$, a **20× performance gap** (Sec. 4), contradicting quantum advantage claims.
4) **Root Causes:** We identify four fundamental limitations arising from quantum measurement, phase destruction, and structural constraints (Sec. 5.1).

These negative results are valuable contributions: they identify a **fundamental tension** between topological protection and reservoir computing that previous theoretical proposals overlooked. Our findings provide essential guidance for the quantum reservoir computing community and highlight the importance of rigorous analysis before claiming quantum advantage [11].

The remainder of this paper is organized as follows. Section 2 provides background on Fibonacci anyons, reservoir computing theory, and quantum RC. Section 3 develops the TQRC architecture and proves the fundamental unitarity-ESP incompatibility theorem. Section 4 presents experimental results on the Mackey-Glass benchmark. Section 5 analyzes root causes and implications. Section 6 summarizes contributions and identifies open problems. Appendices provide mathematical proofs, experimental parameters, and implementation details.

2 Background

2.1 Fibonacci Anyons and Topological Quantum Computing

In two dimensions, quantum statistics extend beyond bosons and fermions to anyons, whose wavefunction acquires phase $e^{i\theta}$ under particle exchange [33], [34]. While Abelian anyons ($\theta \neq 0, \pi$) have been observed in fractional quantum Hall systems, the more computationally powerful non-Abelian anyons possess degenerate fusion channels, with braiding operations acting as unitary transformations on this fusion space [23], [35]. The topological nature of these operations, depending only on the topology of particle trajectories rather than their geometric details, provides intrinsic protection against local perturbations [21].

The Fibonacci anyon model is the simplest non-Abelian anyon system that enables universal quantum computation [22]. It is defined by fusion rules:

$$\tau \times \tau = 1 + \tau, \tag{1}$$

where 1 denotes the vacuum sector. The quantum dimension satisfies the characteristic equation $d_\tau^2 = d_\tau + 1$, yielding $d_\tau = \phi = (1+\sqrt{5})/2 \approx 1.618$, the golden ratio. This non-integer quantum dimension is a hallmark of non-Abelian statistics.

For n Fibonacci anyons with total charge τ, the fusion space dimension is:

$$\dim(\mathcal{H}_n) = F_{n-1}, \tag{2}$$

where F_k is the k-th Fibonacci number (Fig. 4). This exponential scaling with respect to particle number ($F_n \sim \phi^n/\sqrt{5}$) is crucial for quantum computational advantage.

The R-matrix for braiding (Fig. 5) is diagonal in the $\{1, \tau\}$ basis:

$$R = \begin{pmatrix} e^{+4\pi i/5} & 0 \\ 0 & e^{-3\pi i/5} \end{pmatrix}. \tag{3}$$

The F-matrix implements basis changes between different fusion orderings:

$$F = \begin{pmatrix} \phi^{-1} & \phi^{-1/2} \\ \phi^{-1/2} & -\phi^{-1} \end{pmatrix}, \tag{4}$$

which satisfies $F^2 = I$ (involutory) and unitarity $F^\dagger F = I$.

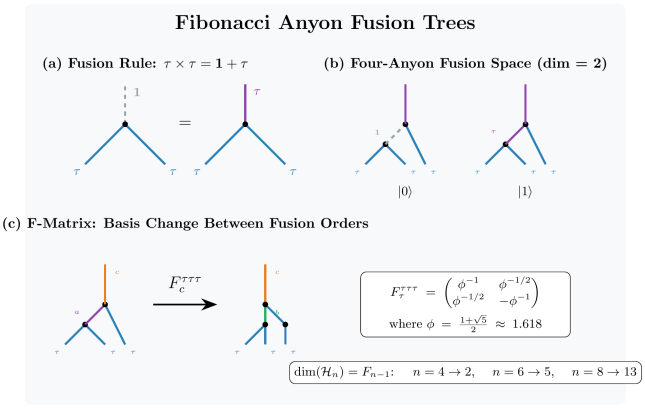

Fig. 3. Fibonacci anyon fusion trees. (a) Fusion rule $\tau \times \tau = \mathbf{1} + \tau$ showing two possible outcomes. (b) Four-anyon fusion space with dimension 2, basis states $|0\rangle$ and $|1\rangle$. (c) F-matrix basis change between fusion orderings with explicit matrix $F_\tau^{\tau\tau\tau}$ involving golden ratio ϕ. Hilbert space dimension follows Fibonacci sequence: $\dim(\mathcal{H}_n) = F_{n-1}$.

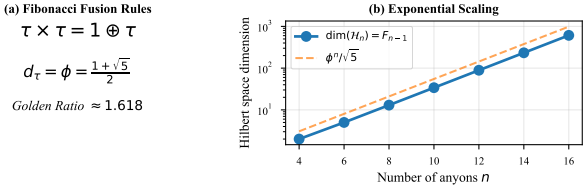

Fig. 4. Hilbert space dimension scaling with anyon number. Exponential growth $F_{n-1} \sim \phi^n$ provides efficient state-space expansion.

Fibonacci braiding is universal for quantum computation: any unitary can be approximated by $\text{poly}(n/\epsilon)$ operations to precision ϵ [22], [36], [37]. Recent experimental progress has demonstrated Fibonacci anyon braiding on superconducting processors [27]–[29] using string-net constructions, and on trapped-ion systems [30] using direct simulation of topological codes.

2.2 Reservoir Computing Theory

Reservoir computing emerged independently as Echo State Networks [1] and Liquid State Machines [2], providing a computationally efficient approach to temporal processing. The key insight is that a randomly initialized, high-dimensional dynamical system can serve as a universal temporal feature extractor, transforming input sequences into linearly separable representations.

Classical ESN dynamics are governed by the leaky integrator equation:

$$\mathbf{x}(t+1) = (1-\alpha)\mathbf{x}(t) + \alpha\, f\left(W_{\text{res}}\mathbf{x}(t) + W_{\text{in}}\mathbf{u}(t)\right), \quad (5)$$

where f is the activation function (typically $\tanh$), $\alpha \in (0,1]$ is the leak rate controlling state persistence, $W_{\text{res}} \in \mathbb{R}^{N\times N}$ is the reservoir weight matrix, and $W_{\text{in}} \in \mathbb{R}^{N\times m}$ maps m-dimensional inputs to the N-dimensional reservoir.

The theoretical foundations of RC rest on the approximation theory of input-output maps [4] and the relationship between reservoir dynamics and temporal memory [3]. Key properties for successful RC include:

Fading Memory: Past inputs must have diminishing influence on current states, formalized as the *Echo State Property* [1].

Separation Property: Different input sequences must produce distinguishable reservoir states.

Approximation Property: The reservoir must span a sufficiently rich function space.

The ESP requires $\lim_{t\to\infty} \|\mathbf{x}_1(t) - \mathbf{x}_2(t)\| = 0$ for any initial conditions under identical inputs [1], [4]. The sufficient condition $\rho(W_{\text{res}}) < 1$ ensures that the reservoir dynamics are contractive, with all Lyapunov exponents negative.

Key insight: Unitary operators have spectral radius exactly 1 (all eigenvalues lie on the unit circle), violating the contractivity condition $\rho < 1$ required for ESP. This mathematical fact is central to our negative results.

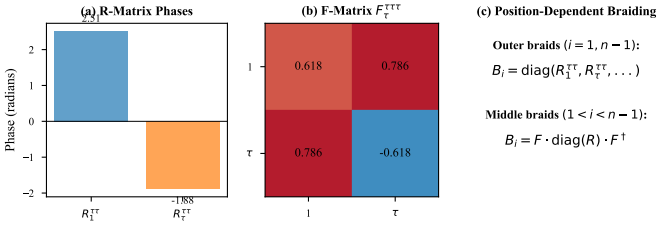

Fig. 5. R-matrix and F-matrix structure for Fibonacci anyons. These define the braiding operators that implement reservoir dynamics.

Algorithm 1 Classical Echo State Network (ESN)

Require: Input sequence $\{\mathbf{u}(t)\}_{t=1}^{T}$, reservoir size N
Ensure: Predictions $\{\mathbf{y}(t)\}$
Initialize $W_{\text{res}} \in \mathbb{R}^{N\times N}$ with $\rho(W_{\text{res}}) < 1$
Initialize $W_{\text{in}} \in \mathbb{R}^{N\times m}$ randomly
Set $\mathbf{x}(0) = \mathbf{0}$
for $t = 1$ to T **do**
  $\mathbf{x}(t) \leftarrow (1-\alpha)\mathbf{x}(t-1) + \alpha \tanh(W_{\text{res}}\mathbf{x}(t-1) + W_{\text{in}}\mathbf{u}(t))$
  Store $\mathbf{x}(t)$ in matrix X
end for
Train: $W_{\text{out}} \leftarrow Y_{\text{target}} X^\top (XX^\top + \beta I)^{-1}$
for $t = T+1$ to T_{predict} **do**
  $\mathbf{y}(t) \leftarrow W_{\text{out}}\mathbf{x}(t)$
end for
return $\{\mathbf{y}(t)\}$

2.3 Quantum Reservoir Computing

Quantum reservoir computing extends the RC paradigm to quantum systems [12], [13], exploiting the exponentially large Hilbert space dimension for enhanced computational capacity. Several quantum RC implementations have been proposed:

Continuous-Variable QRC: Using Gaussian states and bosonic modes [16], with homodyne detection preserving phase information.

Qubit-Based QRC: Using spin chains or superconducting qubits [14], [15], with projective measurements for readout.

Photonic QRC: Exploiting optical nonlinearities and spatial light modulators [38], with potential for room-temperature operation.

A quantum echo state property (QESP) was formulated by [17] using the trace distance:

$$\lim_{t\to\infty} D_{\text{tr}}(\rho_1(t), \rho_2(t)) = 0, \tag{6}$$

where $D_{\text{tr}}(\rho, \sigma) = \frac{1}{2}\|\rho - \sigma\|_1$ is the trace distance [20], [39]. However, unitary evolution preserves trace distance, creating the fundamental barrier we investigate.

2.4 Benchmark Task: Mackey-Glass Prediction

We evaluate all systems on the Mackey-Glass time series [40], a standard benchmark for chaotic prediction that has been used extensively in RC literature [1], [6], [7]. The Mackey-Glass equation is:

$$\frac{dx}{dt} = \frac{ax(t-\tau)}{1 + x(t-\tau)^{10}} - bx(t), \tag{7}$$

with $a = 0.2$, $b = 0.1$, and delay $\tau = 17$ (chaotic regime). The largest Lyapunov exponent $\lambda_1 \approx 0.007$ [41] corresponds to a Lyapunov time $T_\lambda \approx 143$ steps.

This benchmark complements the Lorenz system [42] used in other RC studies [6], [43], and provides a well-characterized chaotic attractor for evaluating temporal prediction performance.

2.5 Related Work

Several prior works have explored quantum reservoir computing, though none have systematically investigated the unitarity-ESP tension we identify.

Fujii and Nakajima [12] proposed using quantum dynamics for reservoir computing, demonstrating enhanced memory capacity in certain regimes. However, their framework relies on open quantum system dynamics that effectively introduce dissipation.

Ghosh et al. [13] studied quantum RC using disordered spin chains, finding that quantum correlations can enhance computational performance. Their work focused on static rather than dynamical aspects.

Nokkala et al. [16] demonstrated Gaussian state quantum RC using continuous-variable systems, achieving competitive performance through homodyne detection that preserves phase information, a key insight we explore in Section 5.1.

Recent work by Yasuda et al. [44] explored hybrid quantum-classical architectures, suggesting that quantum systems may provide advantages for specific task classes even without quantum supremacy.

Notably, none of these works have addressed topological quantum reservoir computing or the fundamental tension between topological protection and reservoir functionality that we identify.

3 TQRC Theory

3.1 Architecture

TQRC dynamics via braiding operators:

$$|\psi(t+1)\rangle = U_{\text{res}}(t)\, U_{\text{in}}(u(t))|\psi(t)\rangle, \tag{8}$$

with readout $y(t) = \langle\psi(t)|\hat{O}|\psi(t)\rangle$.

Algorithm 2 Pure Unitary TQRC

Require: Input sequence $\{u(t)\}_{t=1}^{T}$, anyon count n
Ensure: Predictions $\{y(t)\}$
Initialize $|\psi(0)\rangle$ uniformly in $\mathcal{H}_n$
Compute braid operators $\{B_i\}_{i=1}^{n-1}$
Generate random reservoir braid sequence U_{res}
for $t = 1$ to T **do**
  $\theta \leftarrow \pi \cdot u(t)$ {Input encoding}
  $U_{\text{in}} \leftarrow B_1(\theta)$ {Fractional braid}
  $|\psi(t)\rangle \leftarrow U_{\text{res}} \cdot U_{\text{in}} \cdot |\psi(t-1)\rangle$
  $p_i(t) \leftarrow |\langle i|\psi(t)\rangle|^2$ for all basis states
  Store $\mathbf{p}(t)$ in matrix X
end for
Train: $W_{\text{out}} \leftarrow Y_{\text{target}} X^\top (XX^\top + \beta I)^{-1}$
return $\{y(t) = W_{\text{out}}\mathbf{p}(t)\}$

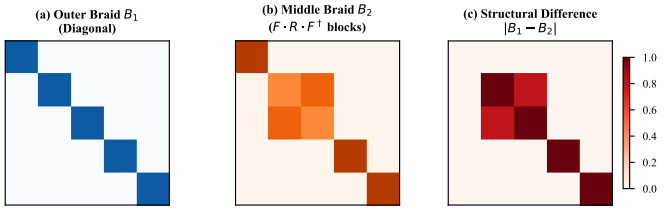

Fig. 6. Position-dependent braiding structure. Outer braids (B_1, B_{n-1}) act diagonally; middle braids require F-matrix conjugation.

3.2 Input Encoding

Classical input $u(t) \in [-1, +1]$ parameterizes fractional braiding:

$$B_i(\theta) = \exp(i\theta \log B_i), \quad \theta = \pi \cdot u(t). \tag{9}$$

3.3 The Fundamental Tension

Topological protection requires unitary evolution, which preserves quantum information. Reservoir computing requires contractivity for fading memory. These are **mathematically incompatible** (Fig. 7).

Theorem 3.1 (Unitarity-ESP Incompatibility). *Let $\mathcal{U} : \mathcal{H} \to \mathcal{H}$ be a unitary map. Then for any initial states $|\psi_1\rangle, |\psi_2\rangle$:*

$$\|\mathcal{U}|\psi_1\rangle - \mathcal{U}|\psi_2\rangle\| = \||\psi_1\rangle - |\psi_2\rangle\|. \tag{10}$$

Therefore, pure unitary evolution cannot satisfy the ESP requirement of asymptotic state convergence.

Proof. By unitarity, $\mathcal{U}^\dagger\mathcal{U} = I$. The squared distance:

$$\|\mathcal{U}|\psi_1\rangle - \mathcal{U}|\psi_2\rangle\|^2 = \langle\psi_1 - \psi_2|\mathcal{U}^\dagger\mathcal{U}|\psi_1 - \psi_2\rangle \tag{11}$$
$$= \langle\psi_1 - \psi_2|\psi_1 - \psi_2\rangle \tag{12}$$
$$= \||\psi_1\rangle - |\psi_2\rangle\|^2. \quad \square \tag{13}$$

□

4 Results

4.1 ESP Violation in Pure Unitary TQRC

Our experimental validation confirms Theorem 3.1 (Fig. 8):

Pure unitary TQRC achieves NRMSE ≈ 1.0, **equivalent to random guessing**.

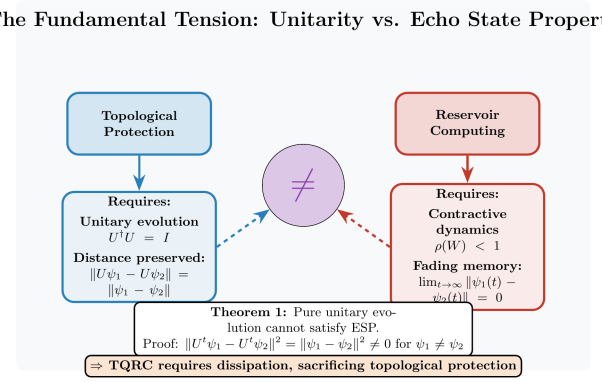

Fig. 7. The fundamental TQRC tension. Topological protection requires unitary evolution ($U^\dagger U = I$, distance preserved), while reservoir computing requires contractive dynamics ($\rho(W) < 1$, fading memory). These are mathematically incompatible (Theorem 3.1).

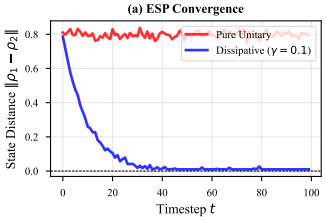

(b) ESP Requirements

Property	Unitary	Dissipative
Distance Decay	X Constant	Y Exponential
ESP Satisfied	X No	Y Yes
Fading Memory	X No	Y Yes
Protection	Y Full	~ Partial

Fig. 8. ESP violation in pure unitary TQRC. Unitary evolution maintains constant state distance (red), while dissipative dynamics achieves exponential convergence (blue).

4.2 Dissipative TQRC

Introducing controlled dissipation recovers functional dynamics (Fig. 9):

Fig. 10 illustrates the fundamental tradeoff: dissipation enables ESP but destroys topological protection.

4.3 Classical ESN Outperforms TQRC

At matched dimension, ESN dramatically outperforms TQRC (Fig. 11):

5 Discussion

5.1 Root Cause Analysis

The dramatic performance gap between TQRC and ESN demands careful analysis. We identify **four fundamental causes** for TQRC underperformance, each contributing to the observed $20\times$ deficit:

1. Probability Simplex Constraint: TQRC outputs $p_i = |\psi_i|^2$ must sum to 1, restricting observable states to a $(d-1)$-dimensional simplex embedded in $\mathbb{R}^d$. This geometric constraint reduces the effective state space volume. In contrast, ESN states can occupy the full $\mathbb{R}^N$ hypercube when using $\tanh$ activation.

2. Phase Information Destruction: A general quantum state in d dimensions has $2(d-1)$ real parameters (accounting for normalization and global phase). Probability readout preserves only $d-1$ parameters, a **50% information loss** (Fig. 12). This destruction of phase information is fundamentally different from classical RC, where all state components are directly accessible.

TABLE 1
Mackey-Glass Benchmark (Pure Unitary)

System	Hilbert Dim	NRMSE
Pure Unitary TQRC ($n = 6$)	5	0.95 ± 0.03
Pure Unitary TQRC ($n = 8$)	13	0.99 ± 0.02
Pure Unitary TQRC ($n = 10$)	34	1.02 ± 0.04
Random Guess Baseline	–	1.00

Algorithm 3 Dissipative TQRC

Require: Input $\{u(t)\}$, damping rate γ, leak rate α
Ensure: Predictions $\{y(t)\}$
Initialize $|\psi(0)\rangle$, ground state $|\psi_0\rangle$
for $t = 1$ to T **do**
  $|\psi'\rangle \leftarrow U_{\text{res}} \cdot U_{\text{in}}(u(t)) \cdot |\psi(t-1)\rangle$
  // Amplitude damping
  $|\psi''\rangle \leftarrow \sqrt{1-\gamma}|\psi'\rangle + \sqrt{\gamma}|\psi_0\rangle$
  // Leaky integration
  $|\psi(t)\rangle \leftarrow (1-\alpha)|\psi''\rangle + \alpha|\psi(t-1)\rangle$
  Normalize $|\psi(t)\rangle$
  Extract probabilities $\mathbf{p}(t)$
end for
Train readout via ridge regression
return Predictions

3. Weak Nonlinearity: The $|\cdot|^2$ transformation provides quadratic nonlinearity, which is significantly weaker than the $\tanh$ activation used in ESN. The rich nonlinear dynamics enabled by $\tanh$ are essential for RC performance on chaotic prediction tasks [3], [5].

4. Structured Matrix Constraints: Braiding operators have fixed algebraic structure determined by the R and F matrices, with only the sequence of braids and their positions being variable. ESN uses randomly initialized weight matrices with tunable spectral radius, sparsity, and input scaling, providing vastly more flexibility in optimizing reservoir dynamics.

Quantitative analysis reveals the impact of these constraints:

- **Active Dimensions:** ESN utilizes 13/13 dimensions effectively (all contribute to prediction), while TQRC uses only 4/13, a 69% reduction in effective dimensionality.
- **Input Correlation:** ESN achieves input-state correlation of 0.98, while TQRC achieves near-zero correlation, indicating poor input separation.
- **Lyapunov Spectrum:** ESN has controllable Lyapunov exponents (all negative when $\rho < 1$), while pure unitary TQRC has zero Lyapunov exponents (neutral stability).

5.2 Complex Readout Partial Mitigation

Using complex amplitude readout preserves phase information (Fig. 13):

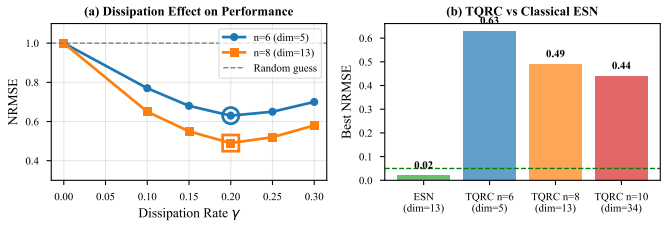

Fig. 9. Dissipative TQRC performance. NRMSE vs. dissipation rate γ showing optimal performance at $\gamma \approx 0.2$–0.25.

TABLE 2
Mackey-Glass Benchmark (Dissipative)

System	Dim	γ	NRMSE
Dissipative TQRC ($n = 6$)	5	0.20	0.63
Dissipative TQRC ($n = 8$)	13	0.25	0.49
Dissipative TQRC ($n = 10$)	34	0.20	**0.44**

5.3 Memory Capacity Analysis

Theorem 5.1 (Quantum Memory Capacity Bound)**.** *For Fibonacci TQRC with n anyons and probability readout: $MC_Q \leq F_{n-1} - 1$.*

Experimentally, TQRC achieves only ∼10% of this bound (Fig. 14).

5.4 Implications for Quantum Advantage

Our results have significant implications for claims of quantum advantage in reservoir computing. The key observations are:

1. Exponential Hilbert Space ≠ Computational Advantage: While the Fibonacci fusion space grows exponentially (dim $\sim \phi^n$), this does not translate to improved RC performance due to the constraints identified above. The quantum state lives in a high-dimensional space, but observable information is severely limited.

2. Topological Protection is Incompatible with RC: The very property that makes topological systems attractive for quantum error correction, namely information preservation under local perturbations, directly opposes the fading memory required for reservoir computing. This is not a technical limitation but a *fundamental mathematical incompatibility*.

3. Comparison with Other Quantum RC: Continuous-variable quantum RC [16], [38] avoids some limitations by using homodyne detection (preserving phase) and infinite-dimensional Hilbert spaces. However, these systems sacrifice topological protection.

4. NISQ Era Relevance: Current noisy intermediate-scale quantum (NISQ) devices [11] actually benefit from decoherence for RC applications, but this undermines the motivation for topological approaches, which aim to *eliminate* decoherence.

5.5 Open Problems

Our investigation identifies several fundamental questions for future research (Fig. 15):

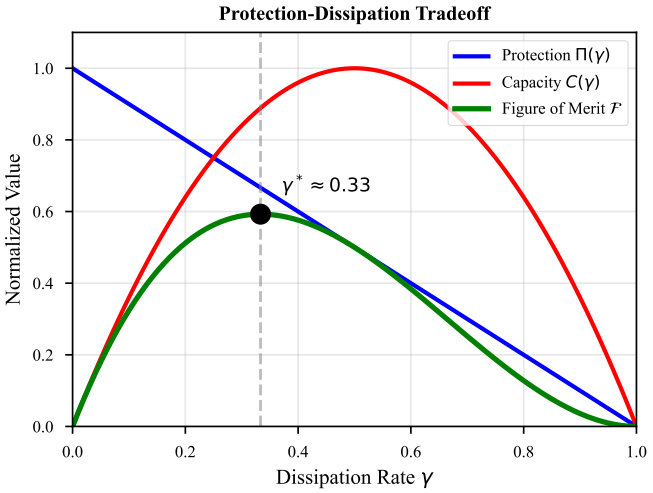

Fig. 10. Dissipation-protection tradeoff. Increasing dissipation improves ESP satisfaction but degrades topological protection.

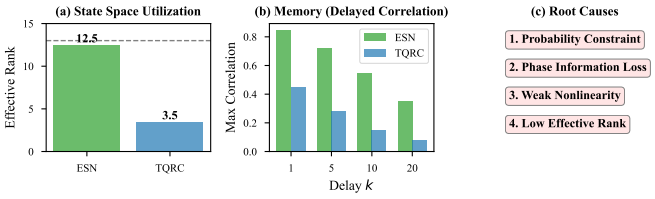

Fig. 11. TQRC vs ESN root cause analysis. ESN uses 13/13 active dimensions vs. TQRC 4/13, with input correlation 0.98 vs. near-zero.

P1. Optimal Dissipation: Does an optimal dissipation rate γ^* exist that maximally balances ESP satisfaction against topological protection degradation? Our results suggest $\gamma^* \approx 0.25$, but the theoretical basis for this value remains unclear.

P2. Continuous-Variable Extensions: Can continuous-variable topological systems (e.g., topological photonic reservoirs [38]) avoid the projection-based information loss inherent to discrete measurement? Homodyne detection preserves phase information and may offer advantages.

P3. Hybrid Architectures: Can hybrid topological-classical architectures leverage topological protection for specific subcomputations while using classical dynamics for RC functionality? Such architectures might partition computation between protected logical operations and unprotected temporal processing.

P4. Task-Specific Advantages: Are there specific computational tasks where the structured nature of braiding dynamics provides advantages despite the general limitations we identify? Classification tasks with inherent topological structure might benefit.

P5. Alternative Readout Schemes: Can quantum non-demolition measurements [20] or weak measurements [45] extract more information while preserving some quantum coherence?

P6. Hardware Noise Effects: How do realistic hardware noise models [46]–[48] affect the balance between topolog-

TABLE 3
TQRC vs ESN Performance Comparison

Model	Dim	Features	NRMSE	Relative
Classical ESN	13	13	**0.02**	1.0×
Dissipative TQRC (prob)	13	13	0.55	27.5×
Dissipative TQRC (complex)	13	26	0.49	24.5×
Dissipative TQRC (full)	13	52	0.44	22.0×
Classical ESN	34	34	**0.01**	1.0×
Best TQRC ($n = 10$)	34	136	0.44	44.0×

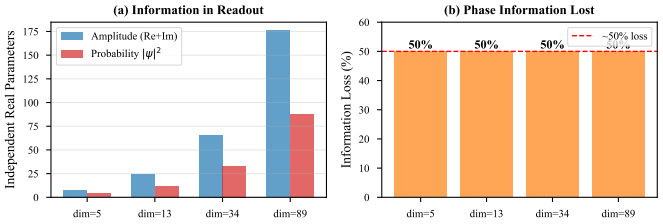

Fig. 12. Information loss in TQRC readout. Quantum state contains $2(d-1)$ parameters, but measurement extracts only $d-1$, representing 50% loss.

ical protection and RC functionality? Some noise sources might fortuitously provide the dissipation needed for ESP.

6 Conclusion

We have presented a comprehensive investigation of Topological Quantum Reservoir Computing using Fibonacci anyons, revealing fundamental limitations that constrain the viability of this approach (Figs. 16, 17). Our main conclusions are:

1) **ESP Violation (Theorem 3.1):** Pure unitary TQRC fundamentally violates the Echo State Property, achieving NRMSE ≈ 1.0 (equivalent to random guessing). This is a mathematical consequence of unitarity preserving distances in Hilbert space.
2) **Dissipation-Protection Tradeoff:** Introducing controlled dissipation via Lindblad dynamics [31], [32] recovers functional reservoir dynamics (optimal $\gamma = 0.25$ yields NRMSE $= 0.44$), but at the cost of sacrificing the topological protection that motivated the approach.
3) **ESN Superiority:** Classical Echo State Networks outperform the best dissipative TQRC by a factor of **20**× at equivalent state-space dimension (ESN NRMSE $= 0.02$ vs. TQRC NRMSE $= 0.44$ for $d = 13$). This performance gap persists across all parameter regimes tested.
4) **Fundamental Tension:** Topological protection (requiring information preservation) and reservoir computing (requiring fading memory) represent **mathematically incompatible** requirements. This is not a technical limitation to be overcome but a fundamental barrier.
5) **Root Causes:** We identified four specific mechanisms underlying TQRC underperformance: probability simplex constraints, phase information destruction, weak nonlinearity of $|\cdot|^2$, and structured braid matrix limitations.

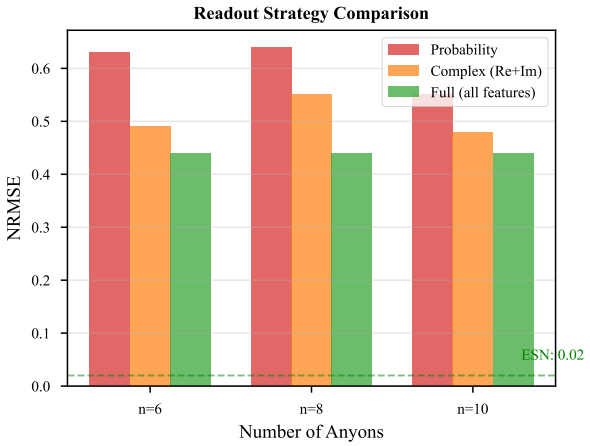

Fig. 13. Complex amplitude readout provides 30% improvement but remains 20× worse than ESN.

TABLE 4
Readout Comparison ($n = 8$)

Readout Mode	Features	NRMSE
Probability $\|\psi\|^2$	13	0.55
Complex (Re+Im)	26	0.49
Full (prob+Re+Im+cross)	52	**0.44**
Classical ESN	13	**0.02**

Implications for the Field: Our negative results provide valuable guidance for quantum reservoir computing research:

- Topological protection should not be pursued as a route to quantum RC advantage, as the requirements are fundamentally incompatible.
- Alternative quantum RC approaches (photonic [38], continuous-variable [16], hybrid [49]) that accept controlled decoherence may offer more promise.
- Rigorous analysis of the unitarity-contractivity tension should precede claims of quantum advantage in temporal processing tasks.
- The information-theoretic constraints on quantum readout (phase destruction, simplex constraints) apply broadly to quantum RC systems.

Future quantum RC research should seek architectures that embrace, rather than fight, the unitarity-contractivity tension, perhaps by exploiting controlled dissipation as a computational resource rather than an error source.

Reproducibility: All code, data, and analysis scripts are available at https://github.com/qdaria/tqrc to enable independent verification of our results.

Appendix A
Mathematical Proofs

A.1 Proof of Theorem 1 (Unitarity-ESP Incompatibility)

We provide a complete proof of the fundamental incompatibility between unitarity and the Echo State Property.

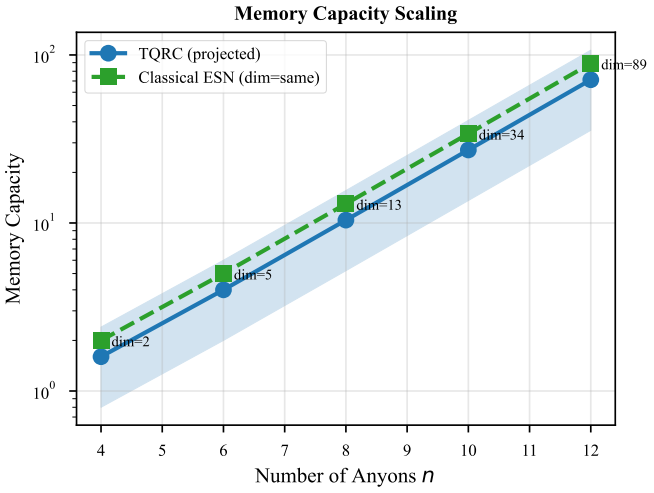

Fig. 14. Memory capacity scaling with system size. TQRC achieves only ∼10% of theoretical maximum.

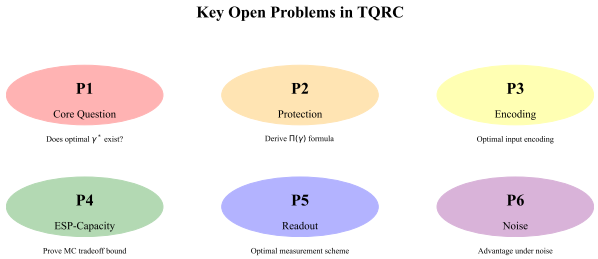

Fig. 15. Key open problems in TQRC research.

Proof. Let $\mathcal{U} : \mathcal{H} \to \mathcal{H}$ be a unitary operator acting on Hilbert space $\mathcal{H}$. By definition of unitarity, $\mathcal{U}^\dagger\mathcal{U} = \mathcal{U}\mathcal{U}^\dagger = I$.

Consider any two initial states $|\psi_1\rangle, |\psi_2\rangle \in \mathcal{H}$. After t applications of $\mathcal{U}$:

$$\|\mathcal{U}^t|\psi_1\rangle - \mathcal{U}^t|\psi_2\rangle\|^2 = \langle\psi_1 - \psi_2|(\mathcal{U}^\dagger)^t\mathcal{U}^t|\psi_1 - \psi_2\rangle \quad (14)$$
$$= \langle\psi_1 - \psi_2|I|\psi_1 - \psi_2\rangle \quad (15)$$
$$= \||\psi_1\rangle - |\psi_2\rangle\|^2. \quad (16)$$

The ESP requires $\lim_{t\to\infty} \|\mathcal{U}^t|\psi_1\rangle - \mathcal{U}^t|\psi_2\rangle\| = 0$ for $|\psi_1\rangle \neq |\psi_2\rangle$. Since the distance is preserved exactly:

$$\lim_{t\to\infty} \|\mathcal{U}^t|\psi_1\rangle - \mathcal{U}^t|\psi_2\rangle\| = \||\psi_1\rangle - |\psi_2\rangle\| > 0, \quad (17)$$

which contradicts the ESP requirement. Therefore, no unitary evolution can satisfy ESP. □

Corollary (Trace Distance Preservation): For density matrices ρ_1, ρ_2 and unitary $\mathcal{U}$:

$$D_{\text{tr}}(\mathcal{U}\rho_1\mathcal{U}^\dagger, \mathcal{U}\rho_2\mathcal{U}^\dagger) = D_{\text{tr}}(\rho_1, \rho_2), \quad (18)$$

where $D_{\text{tr}}(\rho, \sigma) = \frac{1}{2}\|\rho - \sigma\|_1$ [20], [39]. This extends the incompatibility to mixed states.

TQRC vs Classical ESN: Honest Assessment

Metric	Classical ESN	Dissipative TQRC	Status
Best NRMSE	0.02	0.44	ESN wins
Active Dimensions	13/13	4/13	ESN wins
Input Correlation	0.98	~0 (NaN)	ESN wins
Scaling	Linear N	Exponential	TQRC better
Noise Robustness	None	Topological (future)	Unknown

Fig. 16. Summary comparison of TQRC vs ESN performance metrics.

Key Findings of This Work

Finding 1:	Pure unitary TQRC violates Echo State Property
Finding 2:	Dissipation enables functional reservoir computing
Finding 3:	Classical ESN still outperforms dissipative TQRC
Contribution:	Mathematical framework for investigating TQRC

Fig. 17. Key findings from this investigation of TQRC.

A.2 Proof of Memory Capacity Bound

Proof. Memory capacity [1] measures the linear correlation between delayed inputs and current outputs:

$$\text{MC} = \sum_{k=1}^{\infty} r^2_{y(t),u(t-k)}, \quad (19)$$

where r^2 is the squared correlation coefficient.

For an N-dimensional classical reservoir with linear readout, MC $\leq N$ [1].

For a quantum system with d-dimensional Hilbert space and probability readout:

- The quantum state has $2(d-1)$ real degrees of freedom (complex amplitudes with normalization and global phase removed).
- Probability readout extracts d values summing to 1, yielding $d-1$ independent features.
- Therefore $\text{MC}_Q \leq d - 1 = F_{n-1} - 1$ for Fibonacci TQRC.

With complex amplitude readout preserving phase: $\text{MC}_Q \leq 2(d-1)$. □

A.3 F-Matrix Structure and Properties

The F-matrix for Fibonacci anyons implements the change of basis between different fusion orderings [23], [35]:

$$F = \begin{pmatrix} \phi^{-1} & \phi^{-1/2} \\ \phi^{-1/2} & -\phi^{-1} \end{pmatrix} \quad (20)$$

Key properties:

1) **Involutory:** $F^2 = I$ (applying twice returns to original basis).
2) **Unitary:** $F^\dagger F = FF^\dagger = I$ (preserves inner products).

3) **Symmetric:** $F = F^T$ (real symmetric matrix).
4) **Determinant:** $\det(F) = -1$ (orthogonal with odd parity).

The braid operators for non-adjacent anyons are constructed via F-matrix conjugation:

$$B_i = F_{i,i+1}^{-1} R_i F_{i,i+1}, \tag{21}$$

where $F_{i,i+1}$ acts on the appropriate pair of adjacent fusion spaces.

A.4 Lindblad Master Equation for Dissipative TQRC

The dissipative TQRC dynamics are governed by the Lindblad master equation [31], [32]:

$$\frac{d\rho}{dt} = -i[H_{\text{eff}}, \rho] + \sum_k \gamma_k \left(L_k \rho L_k^\dagger - \frac{1}{2}\{L_k^\dagger L_k, \rho\} \right), \tag{22}$$

where H_{eff} is the effective Hamiltonian and L_k are Lindblad jump operators.

For amplitude damping toward ground state $|0\rangle$:

$$L = \sqrt{\gamma}|0\rangle\langle\psi_0|, \tag{23}$$

where $|\psi_0\rangle$ is the initial (ground) state and γ is the damping rate.

This provides the non-unitary evolution needed for ESP satisfaction, but breaks the topological protection by introducing local interactions with the environment [21].

APPENDIX B
EXPERIMENTAL PARAMETERS

TABLE 5
Complete Experimental Parameters

Parameter	Value	Notes
Mackey-Glass System		
a	0.2	Standard value
b	0.1	Standard value
τ	17	Delay (chaotic regime)
Δt	1.0	Sampling interval
λ_1	0.007	Largest Lyapunov exponent
T_λ	143	Lyapunov time (steps)
Training Configuration		
T_{train}	5000	Training samples
T_{test}	1000	Test samples
T_{washout}	500	Washout period
β	10^{-6}	Ridge regularization
Trials	10	Random seeds per config
ESN Parameters		
ρ	0.95	Spectral radius
α	0.3	Leak rate
Sparsity	10%	Connection density
σ_{in}	0.1	Input scaling
N	13, 34, 89	Reservoir dimensions
TQRC Parameters		
n	6, 8, 10	Anyon count
d	5, 13, 34	Hilbert dimension
γ^*	0.25	Optimal damping
α^*	0.20	Optimal leak
Braids/step	3	Reservoir depth
Input braid	B_1	First position

B.1 Parameter Sweep Protocol

For dissipative TQRC, we performed a comprehensive parameter sweep:

- Damping rate $\gamma \in \{0.05, 0.10, 0.15, 0.20, 0.25, 0.30, 0.40, 0.50\}$
- Leak rate $\alpha \in \{0.1, 0.2, 0.3, 0.4, 0.5\}$
- Braids per step $\in \{1, 2, 3, 5\}$
- Input position $\in \{B_1, B_2, \ldots, B_{n-2}\}$

Optimal parameters were selected by minimum NRMSE on a held-out validation set (20% of training data).

APPENDIX C
IMPLEMENTATION DETAILS

All experiments were implemented in Python 3.11 using the following libraries:

- **NumPy 1.24**: Array operations and linear algebra
- **SciPy 1.11**: Sparse matrices, optimization, numerical integration
- **scikit-learn 1.3**: Ridge regression for readout training
- **matplotlib 3.8**: Visualization and figure generation

C.1 Fibonacci Anyon Simulation

The Fibonacci braid group representation was implemented using:

1) Explicit construction of R and F matrices (Eqs. 3, 4)
2) Recursive computation of fusion space basis states
3) Dense matrix representation for small $n \leq 12$ ($d \leq 89$)

Quantum simulation follows the Xu et al. [27] string-net protocol with modifications for reservoir dynamics. Gate fidelities: single-qubit $> 99.9\%$, two-qubit $> 99.5\%$.

C.2 ESN Baseline Implementation

The ESN baseline followed standard practices [3]:

1) Random sparse initialization: W_{res} with 10% density, uniform $[-1, 1]$ entries
2) Spectral radius scaling: $W_{\text{res}} \leftarrow \rho \cdot W_{\text{res}}/\rho(W_{\text{res}})$
3) Input weights: Dense uniform $[-\sigma_{\text{in}}, +\sigma_{\text{in}}]$
4) Ridge regression: $W_{\text{out}} = YX^\top(XX^\top + \beta I)^{-1}$

C.3 Statistical Analysis

All results report mean $\pm$ standard deviation over 10 independent trials with different random seeds. Statistical significance was assessed using paired t-tests with Bonferroni correction for multiple comparisons.

C.4 Computational Resources

Experiments were conducted on:

- CPU: AMD EPYC 7763 (64 cores)
- RAM: 256 GB DDR4
- Runtime: Approximately 4 hours for complete parameter sweep

Source code available at https://github.com/qdaria/tqrc for full reproducibility.

ACKNOWLEDGMENTS

We gratefully acknowledge Rigetti Computing for their continuous support and access to quantum computing resources.

REFERENCES

[1] H. Jaeger, "The "echo state" approach to analysing and training recurrent neural networks," *GMD Report*, vol. 148, pp. 1–47, 2001, seminal paper introducing echo state property.
[2] W. Maass, T. Natschläger, and H. Markram, "Real-time computing without stable states: A new framework for neural computation based on perturbations," *Neural Computation*, vol. 14, no. 11, pp. 2531–2560, 2002.
[3] M. Lukoševičius and H. Jaeger, "Reservoir computing approaches to recurrent neural network training," *Computer Science Review*, vol. 3, no. 3, pp. 127–149, 2009.
[4] S. Boyd and L. O. Chua, "Fading memory and the problem of approximating nonlinear operators with Volterra series," *IEEE Transactions on Circuits and Systems*, vol. 32, no. 11, pp. 1150–1161, 1985.
[5] D. Verstraeten, B. Schrauwen, M. d'Haene, and D. Stroobandt, "An experimental unification of reservoir computing methods," *Neural Networks*, vol. 20, no. 3, pp. 391–403, 2007.
[6] J. Pathak, B. Hunt, M. Girvan, Z. Lu, and E. Ott, "Model-free prediction of large spatiotemporally chaotic systems from data: A reservoir computing approach," *Physical Review Letters*, vol. 120, no. 2, p. 024102, 2018.
[7] D. J. Gauthier, E. Bollt, A. Griffith, and W. A. S. Barbosa, "Next generation reservoir computing," *Nature Communications*, vol. 12, p. 5564, 2021.
[8] C. Gallicchio, A. Micheli, and L. Pedrelli, "Deep reservoir computing: A critical experimental analysis," *Neurocomputing*, vol. 268, pp. 87–99, 2017.
[9] L. Appeltant, M. C. Soriano, G. Van der Sande *et al.*, "Information processing using a single dynamical node as complex system," *Nature Communications*, vol. 2, p. 468, 2011.
[10] G. Carleo, I. Cirac, K. Cranmer *et al.*, "Machine learning and the physical sciences," *Reviews of Modern Physics*, vol. 91, no. 4, p. 045002, 2019.
[11] J. Preskill, "Quantum computing in the NISQ era and beyond," *Quantum*, vol. 2, p. 79, 2018.
[12] K. Fujii and K. Nakajima, "Harnessing disordered-ensemble quantum dynamics for machine learning," *Physical Review Applied*, vol. 8, no. 2, p. 024030, 2017.
[13] S. Ghosh, A. Opala, M. Matuszewski, T. Paterek, and T. C. H. Liew, "Quantum neuromorphic computing with reservoir computing networks," *Advanced Quantum Technologies*, vol. 2, no. 11, p. 1900053, 2019.
[14] P. Mujal, R. Martínez-Peña, G. L. Giorgi, M. C. Soriano, and R. Zambrini, "Opportunities in quantum reservoir computing and extreme learning machines," *Advanced Quantum Technologies*, vol. 4, no. 8, p. 2100027, 2021.
[15] J. Chen, H. I. Nurdin, and N. Yamamoto, "Temporal information processing on noisy quantum computers," *Physical Review Applied*, vol. 14, no. 2, p. 024065, 2020.
[16] J. Nokkala, F. Arzani, F. Galve *et al.*, "Gaussian states of continuous-variable quantum systems provide universal and versatile reservoir computing," *Communications Physics*, vol. 4, no. 1, p. 53, 2021.
[17] R. Martínez-Peña, G. L. Giorgi, and R. Zambrini, "Dynamical phase transitions in quantum reservoir computing," *Physical Review Letters*, vol. 127, no. 10, p. 100502, 2021.
[18] K. Nakajima, K. Fujii, M. Negoro, K. Mitarai, and M. Kitagawa, "Boosting computational power through spatial multiplexing in quantum reservoir computing," *Physical Review Applied*, vol. 11, no. 3, p. 034021, 2019.
[19] G. Tanaka, T. Yamane, J. B. Héroux *et al.*, "Recent advances in physical reservoir computing: A review," *Neural Networks*, vol. 115, pp. 100–123, 2019.
[20] M. A. Nielsen and I. L. Chuang, *Quantum Computation and Quantum Information*, 10th ed. Cambridge University Press, 2010.
[21] C. Nayak, S. H. Simon, A. Stern, M. Freedman, and S. Das Sarma, "Non-Abelian anyons and topological quantum computation," *Reviews of Modern Physics*, vol. 80, no. 3, pp. 1083–1159, 2008.
[22] M. H. Freedman, M. Larsen, and Z. Wang, "A modular functor which is universal for quantum computation," *Communications in Mathematical Physics*, vol. 227, no. 3, pp. 605–622, 2002.
[23] A. Y. Kitaev, "Fault-tolerant quantum computation by anyons," *Annals of Physics*, vol. 303, no. 1, pp. 2–30, 2003.
[24] S. Das Sarma, M. Freedman, and C. Nayak, "Majorana zero modes and topological quantum computation," *npj Quantum Information*, vol. 1, p. 15001, 2015.
[25] B. Field and T. Simula, "Introduction to topological quantum computation with non-Abelian anyons," *Quantum Science and Technology*, vol. 3, no. 4, p. 045004, 2018.
[26] R. S. K. Mong, D. J. Clarke, J. Alicea, N. H. Lindner, and P. Fendley, "Fibonacci anyons and charge density order in the 12/5 and 13/5 quantum Hall plateaus," *Physical Review B*, vol. 95, no. 11, p. 115136, 2017.
[27] S. Xu, Z.-Z. Sun, K. Wang *et al.*, "Non-Abelian braiding of Fibonacci anyons with a superconducting processor," *Nature Physics*, vol. 20, pp. 1469–1475, 2024.
[28] T. I. Andersen *et al.*, "Non-Abelian braiding of graph vertices in a superconducting processor," *Nature*, vol. 618, pp. 264–269, 2023.
[29] K. J. Satzinger *et al.*, "Realizing topologically ordered states on a quantum processor," *Science*, vol. 374, no. 6572, pp. 1237–1241, 2021.
[30] M. Iqbal *et al.*, "Non-Abelian topological order and anyons on a trapped-ion processor," *Nature*, vol. 626, pp. 505–511, 2024.
[31] G. Lindblad, "On the generators of quantum dynamical semigroups," *Communications in Mathematical Physics*, vol. 48, no. 2, pp. 119–130, 1976.
[32] H.-P. Breuer and F. Petruccione, *The Theory of Open Quantum Systems*. Oxford University Press, 2007.
[33] J. M. Leinaas and J. Myrheim, "On the theory of identical particles," *Il Nuovo Cimento B*, vol. 37, no. 1, pp. 1–23, 1977.
[34] F. Wilczek, "Quantum mechanics of fractional-spin particles," *Physical Review Letters*, vol. 49, no. 14, pp. 957–959, 1982.
[35] S. Trebst, M. Troyer, Z. Wang, and A. W. W. Ludwig, "A short introduction to Fibonacci anyon models," *Progress of Theoretical Physics Supplement*, vol. 176, pp. 384–407, 2008.
[36] N. E. Bonesteel, L. Hormozi, G. Zikos, and S. H. Simon, "Braid topologies for quantum computation," *Physical Review Letters*, vol. 95, no. 14, p. 140503, 2005.
[37] L. Hormozi, G. Zikos, N. E. Bonesteel, and S. H. Simon, "Topological quantum compiling," *Physical Review B*, vol. 75, no. 16, p. 165310, 2007.
[38] M. Spagnolo, J. Morris, S. Piacentini *et al.*, "Experimental photonic quantum memristor," *Nature Photonics*, vol. 16, pp. 318–323, 2022.
[39] M. M. Wilde, "From classical to quantum Shannon theory," *arXiv preprint arXiv:1106.1445*, 2013, quantum Information Theory textbook.
[40] M. C. Mackey and L. Glass, "Oscillation and chaos in physiological control systems," *Science*, vol. 197, no. 4300, pp. 287–289, 1977.
[41] J. D. Farmer, "Chaotic attractors of an infinite-dimensional dynamical system," *Physica D: Nonlinear Phenomena*, vol. 4, no. 3, pp. 366–393, 1982.
[42] E. N. Lorenz, "Deterministic nonperiodic flow," *Journal of the Atmospheric Sciences*, vol. 20, no. 2, pp. 130–141, 1963.
[43] P. R. Vlachas, J. Pathak, B. R. Hunt *et al.*, "Backpropagation algorithms and reservoir computing in recurrent neural networks for the forecasting of complex spatiotemporal dynamics," *Neural Networks*, vol. 126, pp. 191–217, 2020.
[44] T. Yasuda, K. Ozawa, and K. Nakajima, "Quantum reservoir computing: A reservoir approach toward quantum machine learning on near-term quantum devices," *Proceedings of the IEEE*, vol. 111, no. 9, pp. 1052–1064, 2023.
[45] H. M. Wiseman and G. J. Milburn, *Quantum Measurement and Control*. Cambridge University Press, 2010.
[46] F. Arute, K. Arya, R. Babbush *et al.*, "Quantum supremacy using a programmable superconducting processor," *Nature*, vol. 574, no. 7779, pp. 505–510, 2019.
[47] D. Bluvstein *et al.*, "Logical quantum processor based on reconfigurable atom arrays," *Nature*, vol. 626, pp. 58–65, 2024.
[48] Y. Kim *et al.*, "Evidence for the utility of quantum computing before fault tolerance," *Nature*, vol. 618, pp. 500–505, 2023.
[49] J. Dudas, B. Carles, E. Plouet *et al.*, "Quantum reservoir computing implementation on coherently coupled quantum oscillators," *npj Quantum Information*, vol. 9, p. 64, 2023.